Using Chaos to Broaden the Capture Range of a Phase-Locked Loop

Elizabeth Bradley

CU-CS-669-93 September 1993

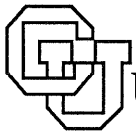

University of Colorado at Boulder
DEPARTMENT OF COMPUTER SCIENCE

Using Chaos to Broaden the Capture Range of a Phase-Locked Loop

Elizabeth Bradley

Department of Computer Science
University of Colorado
Campus Box 430
Boulder Colorado 80309-0430

CU-CS-669-93 September 1993

To appear in the November 1993 issue of the
IEEE Transactions on Circuits and Systems.

Using Chaos to Broaden the Capture Range of a Phase-Locked Loop

Elizabeth Bradley

Abstract — Chaos is common in physical systems, but control engineers have, until very recently, deemed it undesirable and gone to great lengths to avoid it. Such tactics can represent a needless sacrifice in performance — chaos has a variety of useful properties that can significantly enhance engineering designs. In particular, phase-space trajectories on a chaotic attractor densely cover a set of non-zero measure, making all points in that set *reachable* from any initial condition in its basin of attraction. Moreover, the size, shape, and position of the attractor are affected by changes in system parameters, following certain highly characteristic patterns. These properties have been used, in simulations, to broaden the capture range of the common phase-locked loop circuit. An external modulating input is used to throw the unlocked loop into a chaotic regime that overlaps the original capture range. The chaos-inducing modulation is then turned off, allowing the loop's original dynamics to capture the signal. This technique is not limited to this system or even to this branch of engineering; it applies, modulo a few constraints and limitations, to any system that exhibits chaotic behavior and that is subject to design requirements.

1 Introduction

Chaos in phase-locked loops has been recognized and studied for at least a decade. In the late 1970s and early 1980s, researchers investigating chaos in physical systems recognized that, because of isomorphisms in the equations, phase-locked loops could be used to effectively simulate the behavior of driven pendula[7] and Josephson junctions[1], systems that are impractical to explore *in situ* because of difficulties with low speeds or temperatures. Interest in this topic followed in the circuits community several years later[10, 12]. Many other chaotic electronic systems have been discussed in the literature since then, ranging from the venerable Van del Pol oscillator[17] to the well-known Chua's circuit family[28], and culminating in this special issue of the *Transactions on Circuits and Systems.*

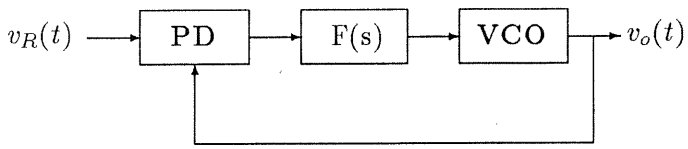

Figure 1: Phase-locked loop block diagram. PD = phase detector, F(s) = low-pass filter, and VCO = voltage-controlled oscillator

More recently, research on chaos in the phase-locked loop has extended beyond analysis to synthesis and actual practical uses of the chaotic behavior. Novel communication schemes[13] based on the phenomenon of synchronized chaos[11, 23] have been used to ensure the security of information transmission. Design improvements in the circuit itself are another practical application. Preliminary results[3, 5] indicate that chaos induced via an external modulating input can increase the capture range of the circuit. This paper refines and expands upon these preliminary results.

The next section sketches the mathematics and theory of operation of the phase-locked loop, with the specific goal of smoothly blending modern nonlinear dynamics and the classic electrical engineer's interpretation of the circuit. Section 3 explains the mechanics of using chaos to broaden the capture range of the circuit. Section 4 explores these ideas and techniques using numerical experiments. Results, caveats, broader implications, and future directions are summarized in the conclusion.

2 Theory and Mathematics of the Phase-Locked Loop

The basic block diagram of the phase-locked loop is shown in figure 1. The phase detector (PD) compares the input *reference signal* $v_R(t) = V_R \sin \omega_R t$ and the output $v_o(t) = V_o \sin(\omega_o t + \phi)$ of the circuit's internal voltage-controlled oscillator or *VCO*. The phase difference between the two signals is measured, filtered, and used to drive the VCO's frequency towards ω_R. The low-pass filter $F(s)$ removes noise, performs loop compensation, and discriminates against unwanted harmonics of the input, to which, in its absence, the loop can lock. Once the circuit is locked to a signal, changes in frequency can be tracked over a *lock range* $\Delta\omega_L$ that is centered on the *free-running frequency* $\omega_\odot$ of the VCO. Initial lock can be acquired over a smaller *capture*

range $\Delta\omega_C$, also centered on $\omega_\odot$.

Most previous implementations of chaotic analog phase-locked loops have employed either mixers or sample-and-hold (S&H) circuits as phase detectors. A simple mixer, multiplying two signals $V_R \sin \omega_R t$ and $V_o \sin(\omega_o t + \phi)$, produces the sum and difference frequencies $\omega_R \pm \omega_o$. If the loop is in lock ($\omega_R = \omega_o$), the sum term — the second harmonic at $2\omega_R$ — is filtered out by the low-pass filter and the output of the PD is $\frac{V_R V_o}{2} K_{pd} \cos\phi$, where K_{pd} is the gain of the phase detector. The mathematics of the sample-and-hold phase detector are more complex. If the reference input is sampled at the VCO's frequency, the output of the S&H contains a term proportional to $\sin\phi$, together with *all* of the harmonics of the sampling frequency ω_o. The hold time of the S&H is 2π over the sampling frequency, so the evenly spaced zeroes on its $\frac{\sin s}{s}$ frequency response occur at the harmonics of ω_o, thereby removing all but the $\sin\phi$ term from the PD's output.

The capture and lock ranges depend in a complicated way on global nonlinear properties of the loop, such as cutoff frequencies and saturation thresholds. When the loop is far from lock and linearization fails, descriptions in the literature are vague and analysis becomes *ad hoc* and/or numerical: "a general expression for loop capture range is not available as the system is highly nonlinear[26]." The exact form of the calculations depends on the dynamics of each of the blocks in figure 1. In practice, the width of the lock range is usually determined by the hard limits of the VCO, but $\Delta\omega_L$ can be further narrowed by signal amplitude reductions *anywhere* in the forward path of the loop: low amplitudes on the reference input V_R or VCO output V_o, low filter cutoff frequency, or a slow or range-limited phase detector. The capture range $\Delta\omega_C$ is always smaller than the lock range and is generally determined by the cutoff frequency ω_{LPF} of the low-pass filter, which is typically set just below the second harmonic of the lowest ω_R to which the loop is expected to lock. The reasoning behind this choice is that if any harmonic of any anticipated reference frequency can pass unattenuated through the filter, the loop can lock to that harmonic instead of to the reference frequency itself[1]. To understand the effects of ω_{LPF} on $\Delta\omega_C$, consider an unlocked loop, where the PD is measuring the phase difference between two unequal-frequency sinusoids. When the frequency of this time-varying phase difference — the $(\omega_R - \omega_o)$ term in the PD's output — is above the filter's rolloff, the feedback loop is effectively broken and none of the correcting signal can be applied to the VCO. Lock and capture range mechanics and dynamics are discussed in more detail later in this section.

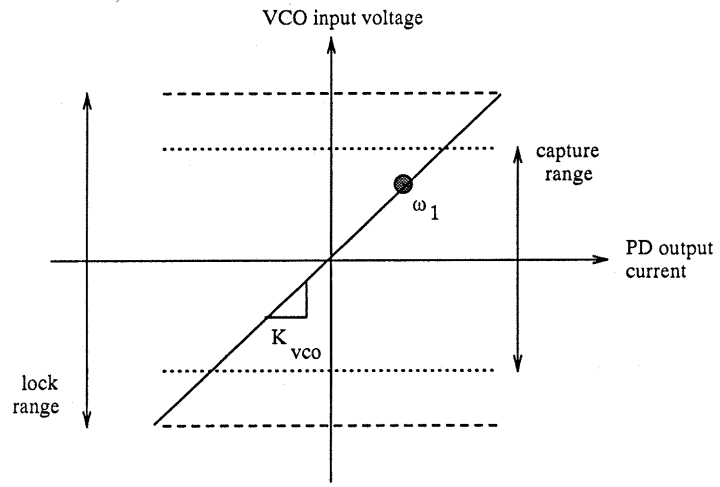

Figure 2: Phase-locked loop characteristics: the shaded point is the equilibrium state of the loop when it is locked to an input frequency ω_1 that is somewhat higher than the center frequency of the VCO. If this frequency changes, the equilibrium state moves along the diagonal line until it reaches the VCO's limits and the loop loses lock

When the loop is locked to an input near the VCO's free-running frequency $\omega_\odot$, the output of the phase detector is small. As the reference frequency ω_R moves away from $\omega_\odot$, the VCO's input — and hence the PD's output — must change for the VCO to track and for the loop to retain lock. This sets up a constant phase offset ϕ_Δ between the input and output signals. In equilibrium, the voltage induced across R_S by the output current of the PD:

$$I_{FB} = \frac{V_o V_R}{2} K_{pd} \cos \phi_\Delta \tag{1}$$

is the DC voltage necessary to drive the VCO's output to ω_R:

$$v_o(t) = V_o \sin(\omega_R t + \phi_\Delta) \tag{2}$$

with

$$\omega_R - \omega_\odot = K_{vco} \frac{V_o V_R}{2} K_{pd} \cos \phi_\Delta \tag{3}$$

These calculations assume unity gain through the loop filter, an accurate approximation if the loop is locked and the phase detector's output is pure DC. The amplitude V_o of the VCO output voltage is also assumed to be constant, independent of ω_o. A diagram of the behavior described by these three equations is shown on figure 2. The axes of the plot are VCO input voltage and phase detector output current. The shaded point represents the system state when the loop is locked to some input frequency ω_1; as ω_1 changes slowly, the point moves along the solid diagonal line whose slope is K_{vco}. If ω_1 were equal to $\omega_\odot$, the shaded point would be at

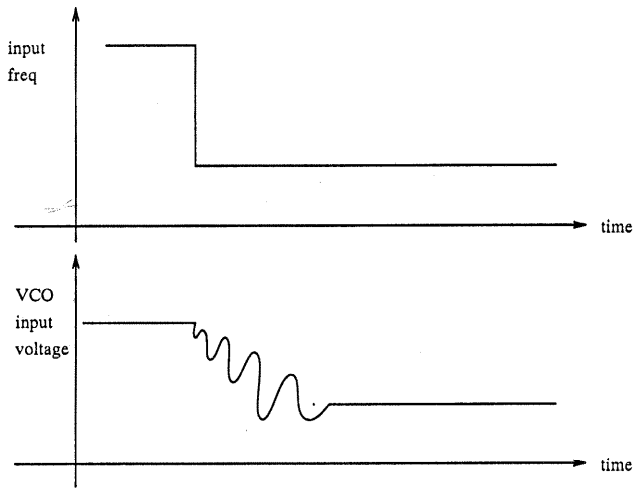

Figure 3: Transient response of a locked loop to an input frequency step that remains within the capture range

the origin. When the frequency difference $\omega_R - \omega_\odot$ exceeds the output range of the VCO — the dashed lines on the figure — the loop loses lock. This range is generally, as discussed in the previous paragraph, a function of the specifications in the VCO's data sheets; it is affected by the supply voltage limits, the dynamic range of the output stage, etc. The dotted capture range limits are narrower, governed by the filter's cutoff frequency via the mechanism described on page 3.

Figure 2 is only valid for slow variations around a locked state. Figure 3 shows a time-domain plot of the transient set off by a *step change* in ω_R — one that does not cause the input to exceed the capture range. The circuit settles to the new equilibrium state via a growing-amplitude (and shrinking frequency) series of cusps. Figure 4 shows, on the same axes as figure 2, the steady-state behavior when ω_R is outside the capture range. The frequency of the time-varying phase difference between input and output far exceeds ω_{LPF} and so the VCO input voltage is zero and $\omega_o = \omega_\odot$. The phase difference oscillates at $\omega_R - \omega_\odot$; the horizontal amplitude of the signal is related only to the constants K_{pd}, V_R, and V_o. If ω_R is lowered to the edge of the capture range, the situation becomes much more complex. The difference frequency $\omega_R - \omega_\odot$ is no longer completely attenuated by the filter, so the VCO input is non-zero, but not large enough to push ω_o all the way to ω_R, even though the latter is theoretically within the VCO's range. The PD's output is swinging far enough, but the filter is breaking the loop. The frequency shortfall propagates back through the phase detector, causing its output to oscillate, which in turn varies the VCO input voltage (since the frequency is now below ω_{LPF}).

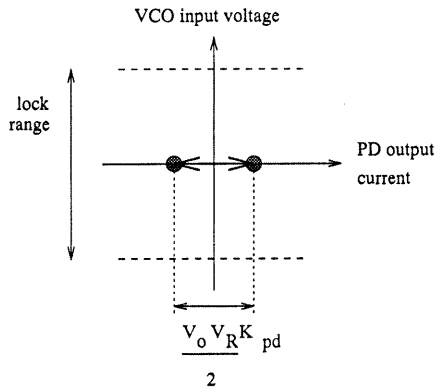

Figure 4: Evolution of the system state when the input frequency exceeds the capture range: $|\omega_R - \omega_\odot| \gg |\frac{\Delta\omega_C}{2}|$. $\omega_\odot$ is the free-running frequency of the VCO

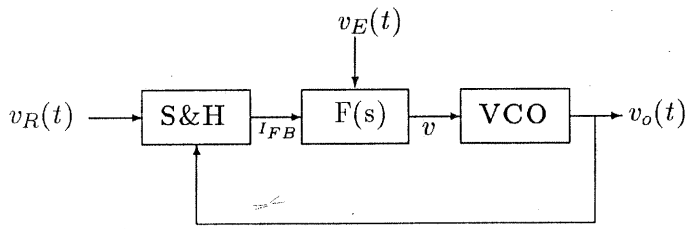

Figure 5: Phase modulator block diagram

A strict interpretation of the dotted-line definition of the capture range on figure 2 is actually somewhat misleading, because the VCO input voltage is really only proportional to $\dot{\phi}$ when ω_R is inside the capture range. Outside this range, the state cannot exceed the dotted limits, which is exactly the range it must reach to attain lock. Note that the effects of the filter are felt directly and indirectly on *both* phase space axes because of the phase shift it introduces above ω_{LPF}. If the loop is to lock to a signal outside $\Delta\omega_C$, the VCO input voltage must be forced outside the dotted boundaries. Effecting this requires adding a *control input* to the circuit.

Figure 5 shows a specialized phase-locked loop circuit with a sample-and-hold PD and an extra input into the filter, which acts as the control input alluded to in the previous paragraph. Electrical engineers traditionally use this circuit to modulate the output phase according to a varying voltage $v_E(t)$. This circuit has uses in other fields as well: it is identical to the one used in [1] and [7] to simulate, respectively, the Josephson junction and the driven pendulum. The next few pages cover the derivation of the equations and describe the correspondences between the different physical systems that they model. These equations will be the basis for the discussion and experiments presented in the rest of this paper.

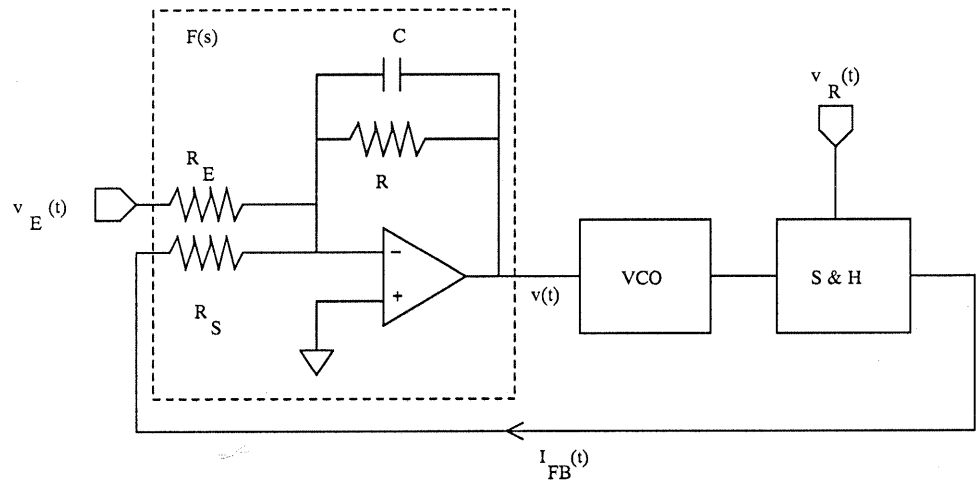

Figure 6: Details of loop compensation and filtering

Figure 6 shows the general form of the operational amplifier circuit used in [1, 7] to perform loop compensation, low-pass filtering, and the addition of the modulating input. $F(s)$ is a simple one-pole low-pass with the transfer function:

$$F(s) = \frac{F_0}{(\frac{s}{\omega_{LPF}} + 1)}; \quad \omega_{LPF} = \frac{1}{RC} \tag{4}$$

In practice, $R \approx R_E = R_S$, so $F_0 \approx 1$.

When the loop is in lock and $\phi \approx 0$, the linearized transfer function (output phase versus input phase) follows the standard second-order form:

$$\frac{\phi_o(s)}{\phi_i(s)} = \frac{1}{(s^2/\omega_{nat}^2) + (2\zeta/\omega_{nat})s + 1} \tag{5}$$

where $\omega_{nat}^2 = \frac{K_{vco}K_{pd}V_R V_o}{2R_S C}$ and the damping constant $2\zeta = \sqrt{\frac{2R_S}{K_{vco}K_{pd}V_R V_o R^2 C}}$. This linearized equation is not useful in the global analysis of this nonlinear system; it is presented here only to define the natural frequency ω_{nat} of the circuit.

The differential equation for the VCO's input $v(t)$ is:

$$C\dot{v}(t) + \frac{v(t)}{R} + \frac{V_R V_o K_{pd}}{2R_S}\sin(\omega_R \tau_o + \phi) = -\frac{v_E(t)}{R_E} \tag{6}$$

The third term reflects the sampling at τ_o, the VCO's period. The sampler fires at the zero crossings of the output sine wave, so the sampled phase is exactly the true phase difference ϕ:

$$(\omega_R \tau_o + \phi) = \phi \tag{7}$$

Since the VCO converts a voltage to a frequency:

$$\dot{\theta}(t) = K_{vco}v(t) \tag{8}$$

Combining equations (6), (7) and (8) yields:

$$\frac{C}{K_{vco}}\ddot{\phi} + \frac{1}{K_{vco}R}\dot{\phi} + \frac{V_R V_o K_{pd}}{2R_S}\sin\phi = -\frac{v_E(t)}{R_E} \tag{9}$$

Clear correspondences exist between equation (9) and the equation of motion for a driven, damped pendulum, with ϕ as the angle of the bob from the vertical:

$$ml\ddot{\phi} + \beta l\dot{\phi} + mg\sin\phi = \frac{\gamma(t)}{l} \tag{10}$$

ω_{nat} in the circuit is equivalent to the natural frequency defined for small oscillations by gravity (g) and the length of the pendulum bob (l):

$$\omega_{nat} = \sqrt{\frac{g}{l}} = \sqrt{\frac{K_{vco}K_{pd}V_R V_o}{2R_S C}} \tag{11}$$

The modulating voltage $v_E(t)$ plays the role of the applied torque $\gamma(t)$. The correspondences for the *critical torque* τ_{crit} and the *damping ratio* $1/Q = \frac{2\beta}{\beta_{crit}}$ are:

$$\tau_{crit} = mgl \tag{12}$$

$$= \frac{R_E V_R V_o K_{pd}}{2R_S} \tag{13}$$

$$1/Q = \frac{2\beta}{2m\sqrt{\frac{g}{l}}} \tag{14}$$

$$= \sqrt{\frac{2R_S}{K_{vco}K_{pd}V_R V_o R^2 C}} \tag{15}$$

The damping ratio is fixed at 1/4 in this paper, as in many of the other studies of this system[6, 7]; this corresponds to a pendulum whose bob loses about two thirds of its amplitude with each swing. This may be observed on the phase portrait for the undriven damped pendulum in figure 7(a), plotted on the axes $\dot{\phi}$ *vs* ϕ. Part (b) of the figure shows system trajectories from the same six initial conditions as part (a), but under the influence of a sinusoidal forcing torque at 1.2 times the critical amplitude and five times the natural frequency of the device. The phase-locked loop equivalent of this well-known phase portrait has the same axes as figure 2 — VCO input voltage $v(t)$ versus PD output current $I_{FB}(t)$ — but with different x-axis scaling, as $I_{FB}(t)$ is actually proportional to $\sin\phi$, not ϕ. However, the additional constraint imposed by the filter implies that the state of the unmodulated circuit can only enter the region between the dotted and dashed lines when a locked input moves out of the capture range.

A similar set of correspondences has been established between the coefficients in equations (9) and (10) and quantities like the quasiparticle pair current in Josephson junctions; see [7] for a full description.

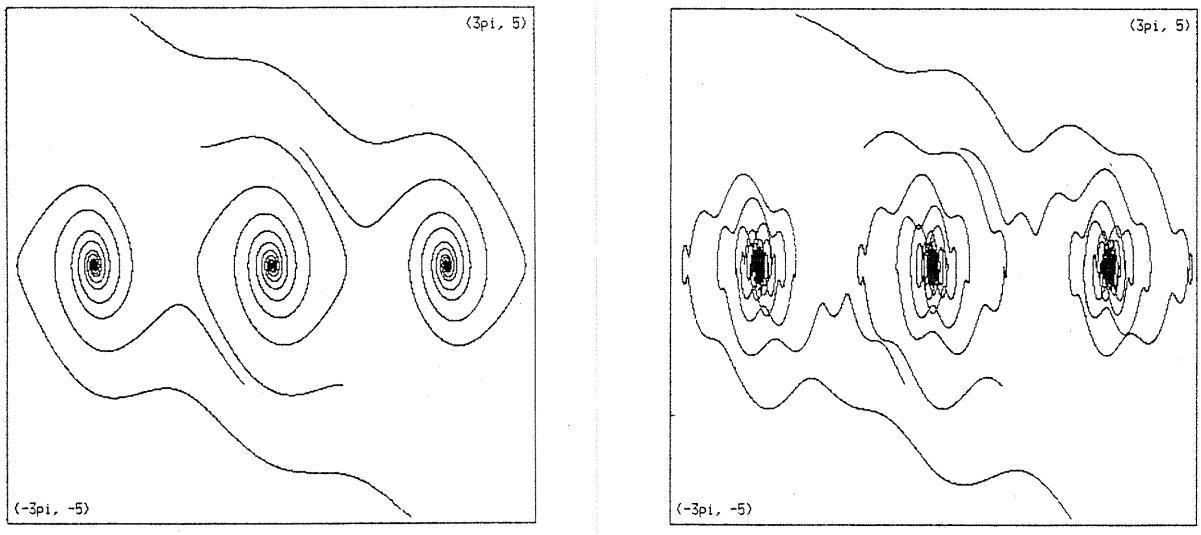

Figure 7: Phase-space trajectories — $\dot{\phi}$ plotted against ϕ — of the driven pendulum: (a) undriven (b) driven at 5 times the device's natural frequency. The same six initial conditions were used in both plots. Damping ratio = 1/4 and applied torque = 1.2 times τ_{crit}

A schematic of the theoretical effects of a small-amplitude sinusoidal modulation $v_E(t)$ applied to the phase-locked loop of figure 5 is shown in figure 8(a). The modulation moves the equilibrium point in an ellipse around the 'locked' state on the diagonal line of figure 2. The vertical component of the ellipse is governed by the derivative of the modulating input $v_E(t)$. The horizontal movement occurs as the phase detector reacts to the v_E-induced change in VCO output frequency; it thus reflects K_{pd} as well. Increases in modulation amplitude cause the ellipse to expand and deform in response to the various nonlinearities in the circuit (see part (b) of the figure). [7] demonstrates that bifurcations occur in this progression, causing

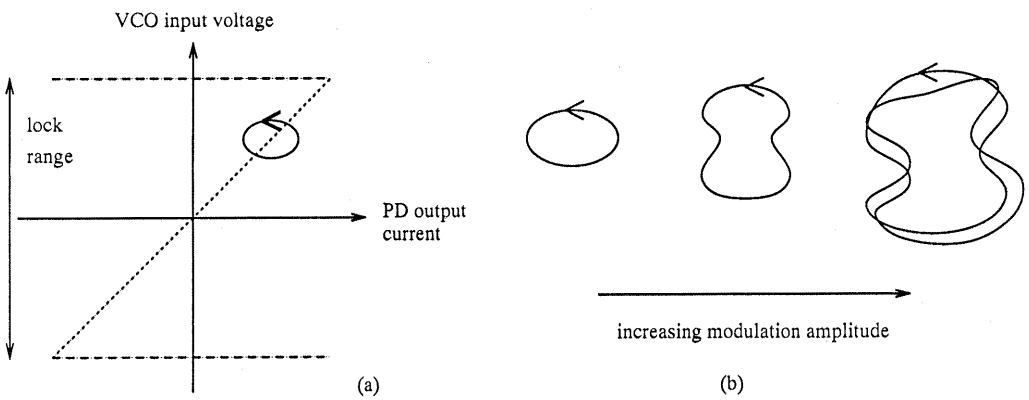

Figure 8: Phase portrait of a modulated loop: (a) small modulation (b) the effects of increasing modulation amplitude

the period-one limit cycle to mutate into a series of higher-order limit cycles, interspersed in some ranges with chaotic attractors. When the amplitude of the modulation is large enough, the edge of the limit cycle touches the dashed lines and the circuit loses lock.

Note that equation (9) incorporates the filter dynamics, and so is valid both inside *and outside* the capture range, as long as the assumptions made in its derivation are not violated. Significant delays in the loop are the most likely and far-reaching cause of failure. A *sampling* phase detector would not, in the face of delays, produce a clean $\sin\phi$ signal because the periodic zeroes on its frequency response would be different from the true harmonics of the sampling frequency. Equation (7) would then fail and the model — equation (9) — would be invalid. A simple mixer, because of the speed of its constituent transistors, would suffer less from this problem. Equation (8) is valid throughout the VCO range, which is assumed to be equivalent to the lock range. At higher frequencies, second-order effects such as op amp slew rate can also cause problems. If any of the assumptions in this paragraph are violated, the resulting unmodeled nonlinearities may cause the behavior of the physical system to differ wildly from the dynamics of equation (9). This issue is discussed further in section 5.

3 Exploiting Chaos

3.1 Theory

The basic idea behind exploiting chaos to change the reachability characteristics of a system is to add a control input and use it to force the trajectories of the augmented system to travel on a chaotic attractor that touches the desired phase-space objective — in this case, the phase-locked loop's capture range. This amounts to finding an input topology and control signal magnitude that, on the axes of figure 2, push the trajectory out of the filter-limited range and up to the voltage and phase levels necessary for the circuit to acquire lock. More precisely, the control objective is the point on the diagonal line that corresponds to the desired locked state and the control input is injected into the modulating input of the phase modulator's filter. Other alternatives exist; for example, one could use a voltage-controlled resistor or capacitor to change the forward path gain or the VCO's center frequency. These tactics may be viewed as causing changes in equation *coefficients*, whereas $v_E(t)$ adds a term to the right-hand side of the equation, changing the topology of the circuit and the dimension of the system.

When the objective is reached, the chaos-inducing input is turned off and the circuit's original dynamics lock on to the signal. Since chaotic attractors are covered densely by trajectories that start in their basins, any such initial condition will eventually evolve to within ϵ of every point on the enclosed attractor, regardless of the size of ϵ. Creating a chaotic attractor that overlaps the capture range thus amounts to making that range *reachable* from any starting condition in its basin. If that basin contains points that are outside the capture range, this constitutes an effective *broadening* of $\Delta\omega_C$. Note that, because it relies upon the circuit's inherent locking dynamics, this particular technique cannot extend the capture range *beyond* the original lock range.

Though chaos's characteristic attractor denseness can be relied upon to bring the trajectory to the objective, *the time taken to do so is effectively nondeterministic.* This is a consequence of the extreme sensitivity of these systems to small perturbations, and is an important drawback of this method. Because of the property elucidated in the shadowing lemma[2], small perturbations do not alter the geometric structure of the attractor, but they *can* affect the order in which its loops are traced out. Thus, one can only make *stochastic* statements, based on ratios of the area of the capture range to the total area of the attractor, about the acquisition time. This implies that chaotically-improved capture range is ineffective when the application requires that lock be achieved, without fail, inside a particular time window. Solutions to this problem — active targeting of a specific point on the attractor, exploiting *sensitive dependence on initial conditions* for control leverage and the cross-sectional eigenstructure on a chaotic attractor for controllability — have been addressed in [5, 24], but practical problems preclude the use of such techniques here[3]. These issues are currently under investigation in the author's group.

3.2 Practice

To broaden the capture range out to the original lock range limits, one must find, for every expected input frequency ω_{R1} that is outside the capture range and inside the lock range, a specific modulating frequency ω_{E1} and amplitude V_{E1} that, acting in conjunction with ω_{R1}, cause the system to become chaotic and the attractor to overlap the equilibrium point $(v_1,\ i_1)$ on the diagonal line of figure 2 that a circuit locked to ω_{R1} would exhibit. When ω_{R1} is detected at the reference input, an external controller modulates the loop at $V_{E1}\sin\omega_{E1}t$ and monitors the state until it nears $(v_1,\ i_1)$. The external modulation is then turned off, allowing the circuit's original dynamics to capture and track the input. Note that the frequency of the

level-shifting, externally induced chaotic component must be below ω_{LPF} for it to have any effect.

On first examination, this would appear to be a complex task, requiring extensive pre-exploration and record-keeping to account for every frequency in the range. However, a chaotic attractor deforms smoothly between bifurcations, so a careful choice of the modulating parameters often suffices for a range of input frequencies. In fact, for some sets of loop parameters, a single set of modulating parameters (V_{E*}, ω_{E*}) takes care of the entire range between $\Delta\omega_C$ and $\Delta\omega_L$. In this case, control would be simple: one would simply turn on the external modulation whenever the loop failed to lock by its natural dynamics. Another potential problem is phase step due to loop delay: even if the VCO frequency is identical to ω_{R1} and the phase difference is the appropriate ϕ_Δ, the PD may not react quickly enough, throwing the loop back out of lock when the controller turns off the external modulation. Some sort of anticipatory control — extrapolation based on derivatives, etc — would easily solve this problem.

Finding V_{E1} and ω_{E1} requires recognition of chaotic attractors and determination of which points they cover. The first of these two tasks presents practical problems; it is often difficult to *prove* that a system is chaotic. Such proofs involve formal mathematical conditions like Smale's "horseshoes"[25] and are impractical with experimental data. A common criterion[15] for diagnosis of chaos in a physical system is the presence of a broad-band power spectrum; other criteria are positive Lyapunov exponents[27], fractal structure[18] in the attractor, positive metric entropy[20], etc.

A recent series of papers on chaos in the phase-locked loop combines several of these criteria. Endo *et al*[10, 12] derive the nonlinear ordinary differential equation of a phase-locked loop demodulator and apply Mel'nikov's method, casting the circuit in the form of a slightly-perturbed Hamiltonian system, to find horseshoes and transverse homoclinic orbits, thus analytically establishing the presence of chaos. This hypothesis — and the correctness of their ODE model — is then verified experimentally with broad-band power spectrum measurements taken from the circuit itself. Similar spectra are used to explore the effects of changes in the modulating frequency, which cause the behavior to bifurcate between chaos and periodicity.

The experiments that follow, in contrast, rely much more heavily on fractal phase-space structure as a diagnostic tool. The circuit involved is a phase *modulator*, rather than a demodulator, and the chaos is treated as a function both of modulating frequency *and amplitude*, as

described at the end of the previous section and pictured in figure 8. The attractor's overlap with the capture range is established visually; this task could be accomplished equally well with electronic sensors and has been automated in a computer program that uses AI-based vision techniques[5].

It should be emphasized that broad-band spectra and fractal phase-space structure are approximate working definitions. They are not rigorous indicators of chaos. More precise definitions are, particularly among mathematicians, the topic of much debate.

4 Experiments

The experiments presented in this section are numerical integrations, performed with an adaptive fourth-order Runge-Kutta algorithm, of equation (9). The plots on the figures have the same axes as figure 2: VCO input voltage versus phase difference. Because of the inherent 2π periodicity on the x-axis, these planar phase portraits are actually unwrapped cylinders, so apparent trajectory crossings do not violate uniqueness constraints. The damping ratio is fixed at 1/4 throughout.

Figure 9 verifies the low-modulation-amplitude phase portrait predicted in figure 8. The frequency is fixed at 0.8 times the natural frequency ω_{nat} — a *modulation frequency ratio* of 0.8 — and the amplitude is varied across the figure, starting at one tenth the critical value defined in equation (12) — a *modulation amplitude ratio* of 0.1 — and ending at a ratio of 1.4. Parts (a) and (b), both plotted for an amplitude ratio of 0.1, show trajectories from several different starting points, all of which relax to the limit cycle near the center of the figure, independent of initial condition, as the input is within the capture range and the modulation amplitude is small enough to not disturb the dynamics. The trajectories can overshoot the limit cycle and loop around inside or outside of it before settling, as in part (b); the precise form of this transient behavior depends strongly on the initial condition. For starting points with high VCO voltage — equivalent to pendula with high velocities — the state can go around the cylinder one or more times in either direction before relaxing to the limit cycle (e.g., the initial condition marked with an 'x' in part (b)). Because of the quotient-space nature of the portraits, differences of $2n\pi$ are immaterial. Parts (c) and (d) of the figure show the effects of raising the modulation frequency. These limit cycles deform and bifurcate with changing amplitude, as on figure 8(b). In figure 9(c), a complex period-three limit cycle, the output

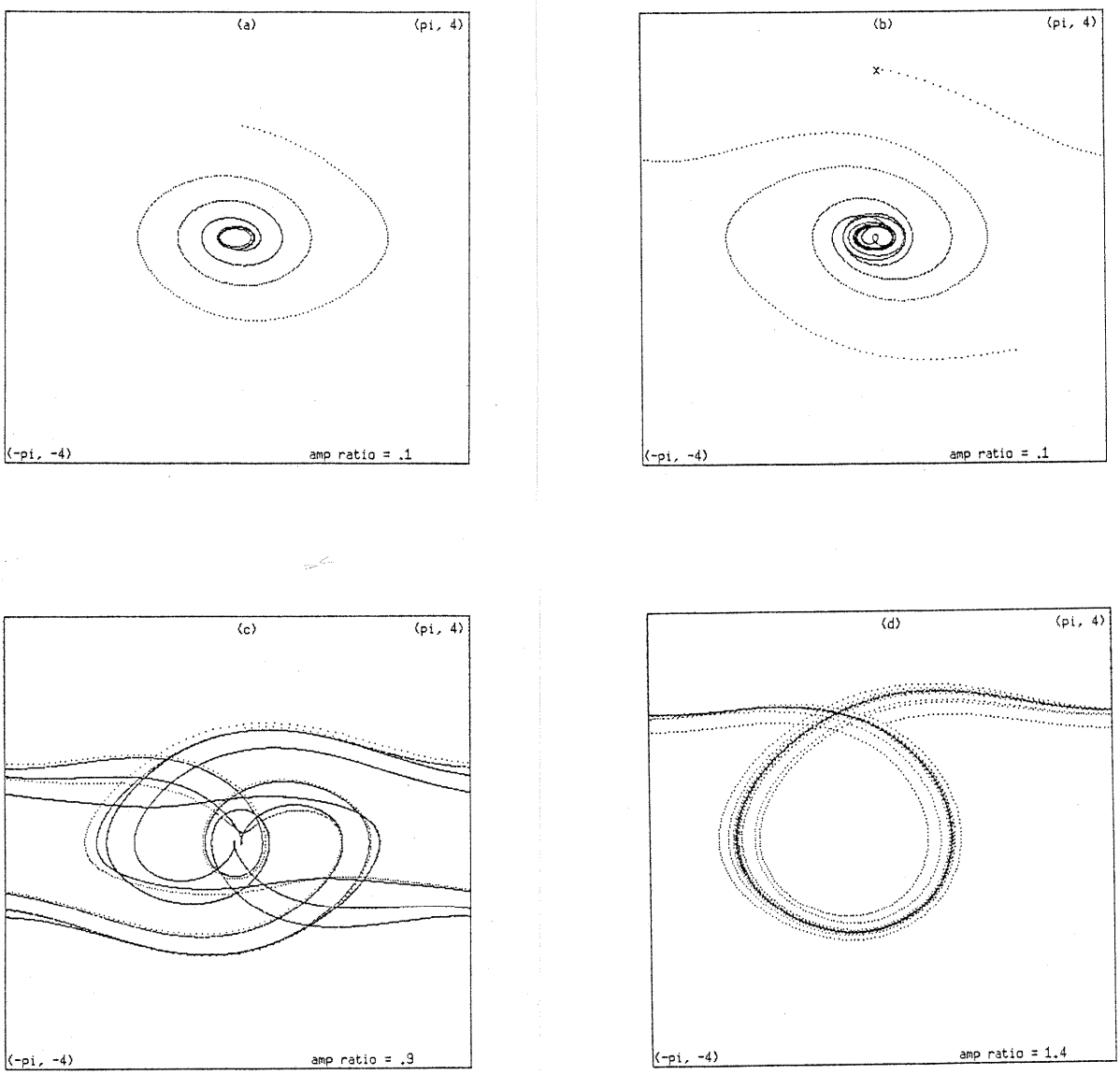

Figure 9: Phase-locked loop trajectories with modulation: the frequency remains constant and the amplitude is raised across the figure. The phase difference on the abscissa is plotted modulo $\pm\pi$; the ordinate is VCO input voltage. The loop finds the same limit cycle — period-one in parts (a) and (b), period-three in part (c) and period-two in part (d) — regardless of initial condition

modulation is locked to the third subharmonic of ω_E. The period-two limit cycle of part (d) is locked to the *second* subharmonic and is offset vertically. In the pendulum, this corresponds to a 'running' solution: the bob goes once over the top, rocks back and forth once at the bottom, then repeats. The circuit, with the modulation imposed in (c) and (d), can no longer strictly be termed a phase modulator, as the output phase is no longer locked to $v_E(t)$. However, the trajectory in part (d) is extremely suggestive: the modulation has caused a vertical offset of the average position of the operating point, and the frequency of the offset component is a *subharmonic* of ω_R. This is exactly the effect that is used to alter the capture range.

Figure 10 shows a progression of *Poincaré sections* over the course of a transition from chaos to order and back to chaos that is induced by variations in ω_E. This sectioning technique, wherein trajectories are sampled once per period of the modulating frequency, reduces the amount of information on the plot while at the same time preserving its structure. This reduction vastly facilitates the recognition of chaotic attractors; figure 11 shows, for comparison purposes, roughly one twentieth of the trajectory whose section appears in figure 10(c). The structure that is readily apparent on the latter is very difficult to recognize in the former. A Poincaré section of a period-one limit cycle like figure 9(a) is a single[4] point, like figure 10(b). The extra three points on the latter are samples of the transient part of the trajectory.

In the experiment pictured in figure 10, the amplitude ratio is fixed at 1.2 and the frequency ratio varies from 0.3 to 0.6. Note the bifurcation from chaos to periodicity that occurs as the modulation frequency is raised from 0.3 ω_{nat} to 0.4 ω_{nat}, and the bifurcation from periodicity back to chaos that occurs between 0.4 ω_{nat} and 0.5 ω_{nat}. Between 0.5 ω_{nat} and 0.6 ω_{nat}, there is no bifurcation and the attractor deforms smoothly. Note, in contrast, the topological differences between the attractors in parts (a) and (c) of the figure, residual evidence of the two (or more) intervening bifurcations.

Since bifurcations are caused by changes in both frequency and amplitude ratios, the information about boundaries between regions of order and chaos in this system is often presented in a two-dimensional *parameter-space portrait*. Figure 12 shows such a portrait for the phase-locked loop. This is a metric space (V_E *vs.* ω_E) plot; it reflects one hundred 30000-time-unit integrations of equation (9) and classification of the resultant behavior according to patterns in the Poincaré sections. Note that only the range below the natural frequency is depicted; above this region, the circuit is periodic. A second reason for disregarding higher frequencies in this

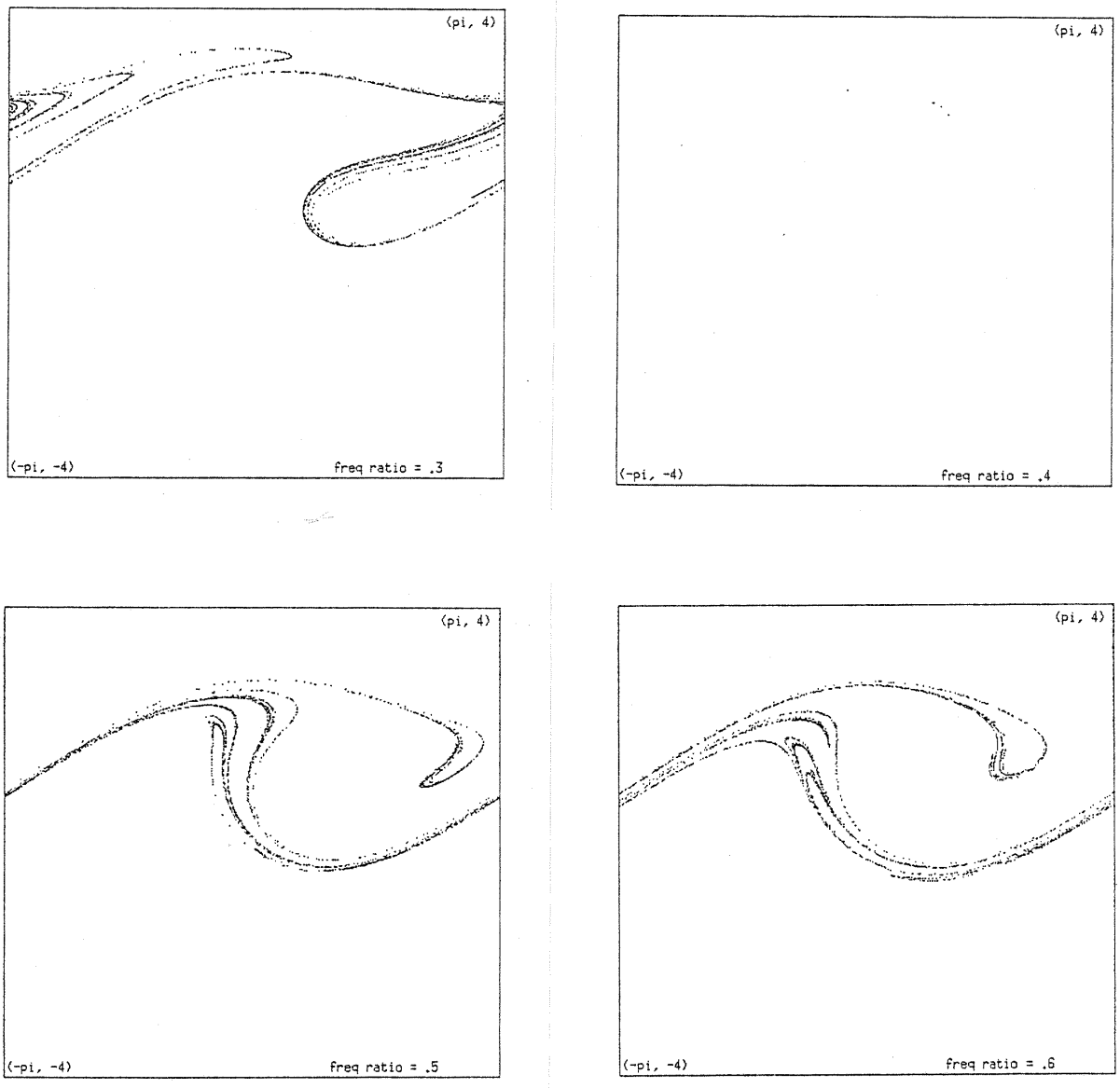

Figure 10: Bifurcations and chaos in the phase-locked loop: (a) chaotic behavior at modulation frequency $\omega_E = 0.3\omega_{nat}$ (b) periodic behavior at $\omega_E = 0.4\omega_{nat}$ (c) chaotic behavior at $\omega_E = 0.5\omega_{nat}$ (d) chaotic behavior at $\omega_E = 0.6\omega_{nat}$. Same axes as the previous figure. Trajectories are sampled once per drive period and ϕ is plotted modulo $\pm\pi$. Damping ratio = 1/4 and modulation amplitude ratio = 1.2

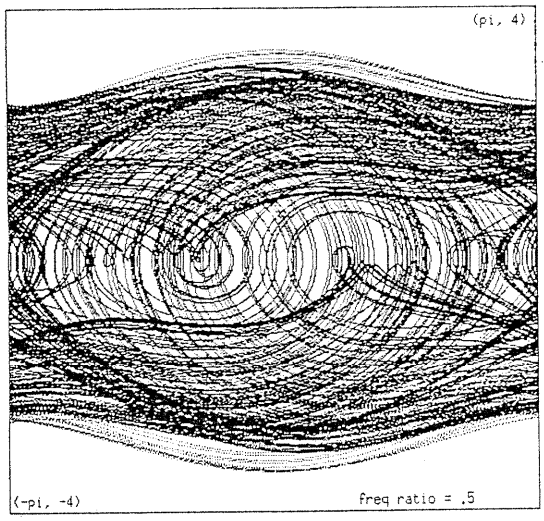

Figure 11: A small segment of the trajectory that was sampled to produce part (c) of the previous figure

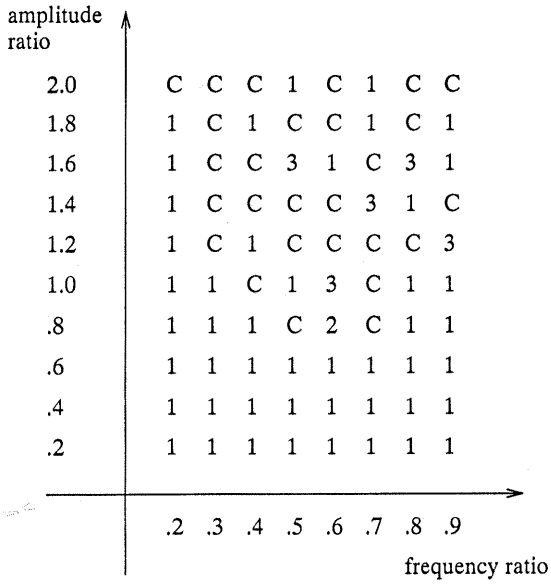

Figure 12: Parameter space portrait of the phase-locked loop. C = chaotic; 1/2/3 = limit cycle with denoted period

experiment is the filter: a frequency whose effects on the output are above ω_{LPF} cannot affect the operation of the loop. For a much more detailed version of this plot, see figure 3 of [7].

Though the exact positions of the boundaries on figure 12 depend on ω_R, the alternating patterns of those boundaries are a common symptom of dissipative chaotic systems. These patterns are used here as first-order guidelines in the search for the modulation parameters V_{Ei} and ω_{Ei} that give rise to the chaotic attractors that broaden the circuit's capture range. Specifically, for each ω_{Ri}, the search begins with a low-amplitude drive at the natural frequency and proceeds downwards in frequency. If no encounter with a periodic/chaotic boundary occurs, the amplitude is raised and the process is repeated. Once a chaotic attractor is found, its intersection with the capture range is determined and the effects of small changes in amplitude and frequency ratios are assessed (e.g., the attractor in the range explored in figure 10(c)—(d) moves down and to the left as ω_E is increased.) If the attractor is close to but does not intersect the capture range, those local effects are exploited to find parameter values that make the intersection non-zero. This type of exploration — though with a somewhat different search pattern — was mechanized and automated by the AI program *Perfect Moment*[3, 4, 5] that was mentioned in the penultimate paragraph of section 3.2.

This exploration and its results are demonstrated in the series of portraits in figure 13. The bounds and slopes — the horizontal lines that define the capture range and the diagonal line the represents the locus of locked states — reflect one set of design choices for ω_{LPF}, K_{VCO}, etc. The objective, shown as a small cross on the diagonal line, is outside this capture range. The experiment consists of finding a chaotic attractor that overlaps this point. The initial phase of the exploration — the first-cut search for chaotic behavior — is omitted from this figure; the study of attractor movement near and coverage of the objective is depicted in some detail. Like figure 10, these plots show Poincaré sections rather than full trajectories; note that only a rough sampling of points on the attractor gives an adequate idea of its coverage. The [amplitude ratio, frequency ratio] = [1.6, 0.3] attractor in part (a) does not quite touch the objective. Raising the frequency ratio moves the attractor down and away from the objective; see part (b). Raising the *amplitude* ratio moves the attractor towards and then past the cross; see parts (c) and (d). The range between these last two plots — amplitude ratio 1.8 to 2.0 — is then examined in more detail to determine the precise parameter values [1.9, 0.3] that cause overlap to occur. A magnified view of the section of this attractor that falls near the objective is shown in figure 14. Note that the intersection of the attractor and the diagonal

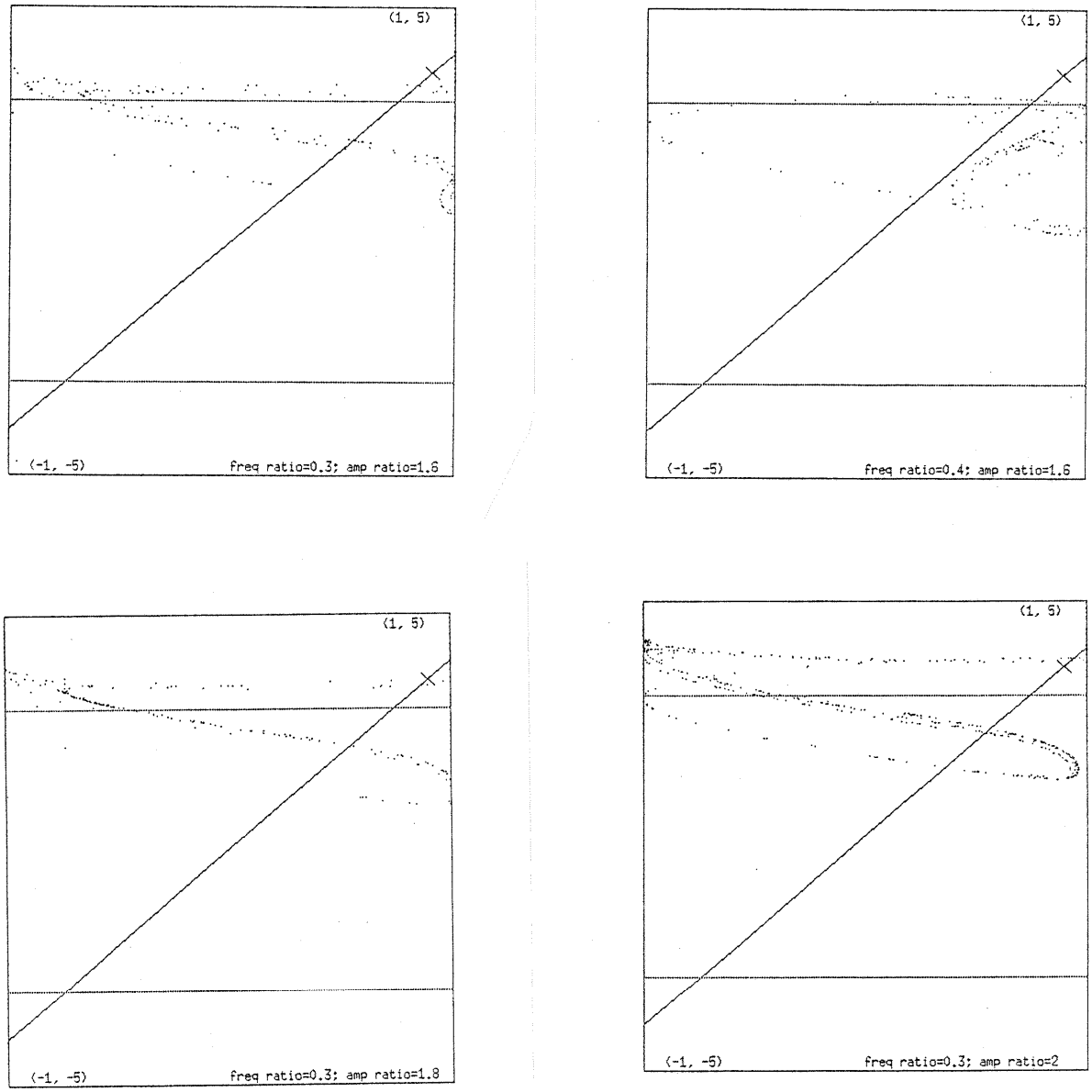

Figure 13: Searching for a chaotic attractor that broadens the capture range: unlike the previous figures, the x-axis here is proportional to $\sin\phi$. The capture range is indicated by the two horizontal lines. The Poincaré section of the [amplitude ratio, frequency ratio] = [1.6, 0.3] attractor in part (a) does not quite touch the objective — the cross on the diagonal line. Raising the frequency ratio moves the attractor down and away from the objective; see part (b). Raising the amplitude ratio moves the attractor towards — part (c) — and then past (part (d)) the cross. The parameter range between parts (c) and (d) is next examined more closely to determine the precise values that cause overlap to occur

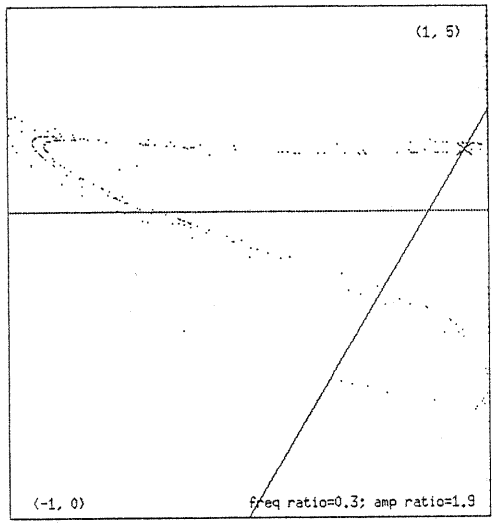

Figure 14: The chaotic attractor found as a result of the search: amplitude ratio = 1.9 and frequency ratio = 0.3. The intersection of this attractor with the diagonal line that represents the locus of locked states surrounds the objective, making it — *and the range of frequencies that surrounds it* — reachable

line is a Cantor set, so the "overlap" may not withstand closer examination. However, solving this problem would simply require a more exhaustive search of the parameter range because the chaotic attractor deforms smoothly therein as the amplitude ratio is varied.

This attractor exhibits all the properties and features discussed in section 3. It arises from the combination of a reference input that is outside the capture range and a control input that is specifically chosen to cause the system state to move on a chaotic attractor that overlaps the objective. The amplitude and frequency ratios of this modulating control input can be used by an external controller to enable the loop to capture this reference frequency. This type of exploration can be extended to other frequencies as well; note the smooth movement of the attractor's intersection with the diagonal line as the parameters are varied. Finally, this intersection is a Cantor set, not a point, so one set of parameters can suffice for a *range* of input frequencies: all that fall within the extended overlap region. The width and spacing of this region can also be controlled with the bifurcation parameters, further extending the power of the technique; via a straightforward extension of the exploration/coverage techniques described here.

5 Conclusions

This paper proposes and describes a new design technique that uses chaos to selectively make phase-space points *reachable* and presents numerical experiments that verify the results. In the specific example used to demonstrate this technique — the phase-locked loop — a chaotic attractor is used to broaden the circuit's *capture range*. An external modulating input is used to throw the unlocked loop into a chaotic regime that overlaps the original capture range. The chaos-inducing modulation is then turned off, allowing the loop's original dynamics to capture the signal. This technique is *not* a universal panacea for control. It cannot make all points reachable, only those that can be covered by a chaotic attractor for some reasonable control topology and parameter value. Classic control theory can be viewed as the search for and stabilization of a fixed point near the objective. Intuitively, it seems obvious that finding an overlap between a set of non-zero measure (a chaotic attractor) and a single point is easier than attempting to superimpose two points — the classic approach[5].

Though these results are promising, equation (9) may not be a good model, so definitive verification can only be drawn from physical experiments. These are in progress in the author's research group, using a commercial phase-locked loop IC in order to foster reproducibility. A variety of assumptions are implicit in the mathematical development of section 2: that the reference input, modulating input, and VCO output are pure tones at fixed amplitudes, that the PD is effectively linear in the VCO's range, and so on. If any of these fail, the model is inaccurate, which is particularly problematic here because chaos is highly sensitive to parameters — equation coefficients — as well as to initial conditions. However, the effects exploited in this paper — bifurcations, densely-covered chaotic attractors that move and change shape as parameters are varied, etc — are *generic* and have been amply demonstrated in physical experiments, both in the phase-locked loop[1, 7, 10, 12] and in a wide variety of other systems. This demonstrated corroboration of the physical properties upon which this technique rests strongly suggests that its simulated results will extend smoothly to physical systems.

The underlying novel concept in this paper is that intentional use of chaos to change the design parameters of an existing system is a powerful — and heretofore neglected — technique. This thread of research was initiated by work on a computer program, *Perfect Moment*, that autonomously explores chaotic dynamic systems and designs controllers that exploit the unique attributes of chaotic behavior[5]. In the particular example used in this paper, chaos is not

the only, nor, arguably, even the best way to attain the design goals and force the capture range to include a particular frequency. In fact, if that frequency were known in advance, one could simply design the loop around it at the outset. Another caveat is the nondeterministic nature of the acquisition time, discussed on page 11. A more general problem is observability: this technique can only be used if the system state is either directly or indirectly accessible[6]. Despite these drawbacks, this design approach appears to be quite successful. It provides a possible solution when, for example, a set of design criteria are for the most part easy to meet, but are vastly complicated by one outlying requirement. Consider a loop that must acquire lock very quickly, with no overshoot, in a small range of medium frequencies, and that must *also* lock to some other, much smaller, frequency, *with acquisition time being of little consequence.* In this case, one might design the loop around the first cluster of requirements using standard techniques, then employ intentionally-induced chaos to bring in the outlying point[7].

The method can also be extended, beyond alteration of the global convergence properties of the system and the reachability of particular objectives, to optimization. Traditional control avoids chaotic regions; opening up those regions to consideration and use can only improve the 'cost' of the reference trajectory. A direct path through a chaotic region, rather than a circuitous one around its perimeter, can be faster and shorter. If one axis of the phase space corresponds, for example, to the fuel consumption of an aircraft, the advantages of a shorter path are obvious. These effects were also explored in the research on the program *Perfect Moment.*

The work presented in this paper ties into the broader field of *controlling chaos*, which has developed into a hotbed of theoretical and applied research in the past three or four years[2, 21], even leading to practical engineering applications. One implemented and tested example is the stabilization of the unstable periodic orbits embedded within a magnetoelastic ribbon's chaotic attractor[8]. Besides the stabilization of these orbits, recent developments in this field have included the use of chaos's symptomatic *sensitive dependence on initial conditions* as control leverage[4, 24], mentioned in section 3.1 as a potential solution to the acquisition time problem. This sensitivity is not only a source of leverage, but also of exponential magnification of control errors, so additional control is required to track any chaotic reference trajectory. Nonlinear dynamics theory gives some qualitative information about the eigenvectors and eigenvalues on a chaotic attractor, and hence the number of control inputs required to accomplish the tracking task. For example, a three-dimensional chaotic attractor has one unstable and one

stable eigenvector in cross section. Stabilizing and point with respect to the cross section thus requires only one control signal. This feature is used in both [5] and [21] to stabilize the state once it reaches the control objective, and in the latter to recover from tracking errors along the path as well.

The technique described in this paper applies to any system that exhibits chaotic behavior and is subject to design requirements. As mentioned above, it cannot make all points reachable, but it does provide a powerful new tool for a designer's arsenal. Like any other technique, it has advantages and drawbacks. All of the latter — and some of the former — stem from sensitivity to parameter and state changes. Designs that derive control leverage from this sensitivity must also account for exponential error growth, either via additional control, as discussed in the previous paragraph, or by relying on denseness and the shadowing lemma — two of the method's advantages — and living with nondeterministic acquisition times.

Though the tactics described here are emphatically inappropriate for nuclear plants and other systems where the time to attain control or the consequences of failure are critical, controlled chaos has a vast array of potential applications, arising in all branches of engineering: fluid flow[22], chemical reactions[16], robot movement[14], air, space, and ground vehicles[19], etc. Chaos is ubiquitous and many of its properties are universal; design techniques that intelligently exploit this physical behavior, rather than avoid it, have the potential to be broadly applicable as well as extremely powerful.

References

[1] C. K. Bak and N. F. Pedersen. Josephson junction analog and quasiparticle-pair current. *Applied Physics Letters*, 22:149–150, 1973.

[2] A. M. Bloch and J. E. Marsden. Controlling homoclinic orbits. *Theoretical and Computational Fluid Mechanics*, 1:179–190, 1989.

[3] E. Bradley. A control algorithm for chaotic physical systems. In *First Experimental Chaos Conference*. World Scientific, 1991.

[4] E. Bradley. Control algorithms for chaotic systems. In G. Jacob and F. Lamnabhi-Lagarrigue, editors, *Lecture Notes in Control and Information Sciences*, volume 165, pages 307–325. Springer-Verlag, Paris, December 1991.

[5] E. Bradley. *Taming Chaotic Circuits*. PhD thesis, M.I.T., September 1992.

[6] P. J. Bryant and J. W. Miles. On a periodically forced, weakly damped pendulum. Part I: Applied torque. *Journal of the Australian Mathematical Society*, 32:1–22, 1990.

[7] D. D'Humieres, M. R. Beasley, B. Huberman, and A. Libchaber. Chaotic states and routes to chaos in the forced pendulum. *Physical Review A*, 26:3483–3496, 1982.

[8] W. L. Ditto, S. N. Rauseo, and M. L. Spano. Experimental control of chaos. *Physical Review Letters*, 65:3211, 1990.

[9] J.-P. Eckmann. Roads to turbulence in dissipative dynamical systems. *Reviews of Modern Physics*, 53:643–671, 1981.

[10] T. Endo and L. O. Chua. Chaos from phase-locked loops. *IEEE Transactions on Circuits and Systems*, 35:987–1003, 1988.

[11] T. Endo and L. O. Chua. Synchronization of chaos in phase-locked loops. *IEEE Transactions on Circuits and Systems*, 38:1580–1588, 1991.

[12] T. Endo, L. O. Chua, and T. Narita. Chaos from phase-locked loops — part II, non-Hamiltonian case. *IEEE Transactions on Circuits and Systems*, 36:255–263, 1989.

[13] J. Gullicksen, M. de Sousa Vieira, M. A. Lieberman, R. Sherman, A. J. Lichtenberg, J. Y. Huang, W. Wonchoba, M. Steinberg, and P. Khoury. Secure communications by synchronization to a chaotic signal. In *First Experimental Chaos Conference*. World Scientific, 1991.

[14] J. Hodgins and M. Raibert. Biped gymnastics. *International Journal of Robotics*, 9:115, 1990.

[15] B. A. Huberman and A. B. Zisook. Power spectrum of strange attractors. *Physical Review Letters*, 46:626–628, 1981.

[16] J. L. Hudson and J. C. Mankin. Chaos in the Belousov-Zhabotinskii reaction. *Journal of Chemical Physics*, 74:6171–6177, 1981.

[17] M. P. Kennedy and L. O. Chua. Van der Pol and chaos. *IEEE Transactions on Circuits and Systems*, 33:974–980, 1986.

[18] B. B. Mandelbrot. *The Fractal Geometry of Nature*. Freeman, New York, 1983.

[19] J. E. Marsden, O. M. O'Reilly, F. J. Wicklin, and B. W. Zombro. Symmetry, stability, geometric phases, and mechanical integrators. *Nonlinear Science Today*, 1:4–21, 1991.

[20] G. Mayer-Kress, editor. *Dimensions and Entropies in Chaotic Systems.* Springer, Berlin, 1985.

[21] E. Ott, C. Grebogi, and J. A. Yorke. Controlling chaos. *Physical Review Letters*, 64:1196–1199, 1990.

[22] J. M. Ottino. *The Kinematics of Mixing: Stretching, Chaos, and Transport.* Cambridge, Cambridge U.K., 1992.

[23] L. M. Pecora and T. L. Carroll. Synchronization in chaotic systems. *Physical Review Letters*, 64:821–824, 1990.

[24] T. Shinbrot, E. Ott, C. Grebogi, and J. A. Yorke. Using chaos to direct trajectories to targets. *Physical Review Letters*, 65:3215, 1990.

[25] S. Smale. Differentiable dynamical systems. *Bulletin of the American Mathematical Society*, 73:747–817, 1967.

[26] J. Smith. *Modern Communication Circuits.* McGraw-Hill, New York, 1986.

[27] A. Wolf. Quantifying chaos with Lyapunov exponents. In *Chaos*, pages 273–290. Princeton University Press, Princeton NJ, 1986.

[28] S. Wu. Chua's circuit family. *Proceedings of the IEEE*, 75:1022–1032, 1987.

Footnotes

---

[0]Manuscript received _____. The author is with the Department of Computer Science and the Department of Electrical and Computer Engineering at the University of Colorado, Boulder, CO 80309-0430. This report describes research done at the Artificial Intelligence Laboratory of the Massachusetts Institute of Technology. Support for the laboratory's artificial intelligence research is provided in part by the Advanced Research Projects Agency of the Department of Defense under Office of Naval Research contracts N00014-85-K-0124 and N00014-86-K-0180. The author was also supported in part by an AAUW dissertation fellowship.

[1]A tradeoff arises here between speed and discrimination: lowering ω_{LPF} may preclude harmonic locking, but it also slows the response time of the loop and lenghtens acquisition time.

[2]This lemma can be informally stated "with high probability, the sample paths of the problem with external noise follow *some* orbit of the deterministic system closely[9]."

[3]The trajectories are so long that exponential divergence maps quantization-error-level noise up to the signal level, precluding any possibility of control.

[4]or pair of points, depending on the definition that is used.

[5]This naive argument neglects the region of control around the target point because its effects are identical in both cases.

[6]This limitation is common, but not universal, in control systems. Observability is a tighter criterion than controllability; some systems can be controlled using only output feedback and no information about the state.

[7]Again, there are other ways to do this: a switched-capacitor network or voltage-controlled resistor could be used to adapt the bandwidth of the loop filter to the sensed input frequency. Inducing chaos through the modulating input is simply a new and conceptually different design technique that accomplishes these goals.

Figure and Table Captions

Fig. 1. Phase-locked loop block diagram. PD = phase detector, F(s) = low-pass filter, and VCO = voltage-controlled oscillator.

Fig. 2. Phase-locked loop characteristics: the shaded point is the equilibrium state of the loop when it is locked to an input frequency ω_1 that is somewhat higher than the center frequency of the VCO. If this frequency changes, the equilibrium state moves along the diagonal line until it reaches the VCO's limits and the loop loses lock.

Fig. 3. Transient response of a locked loop to an input frequency step that remains within the capture range.

Fig. 4. Evolution of the system state when the input frequency exceeds the capture range: $|\omega_R - \omega_\odot| \gg |\frac{\Delta\omega_C}{2}|$. $\omega_\odot$ is the free-running frequency of the VCO.

Fig. 5. Phase modulator block diagram.

Fig. 6. Details of loop compensation and filtering.

Fig. 7. Phase-space trajectories — $\dot{\phi}$ plotted against ϕ — of the driven pendulum: (a) undriven (b) driven at 5 times the device's natural frequency. The same six initial conditions were used in both plots. Damping ratio = 1/4 and applied torque = 1.2 times τ_{crit}.

Fig. 8. Phase portrait of a modulated loop: (a) small modulation (b) the effects of increasing modulation amplitude.

Fig. 9. Phase-locked loop trajectories with modulation: the frequency remains constant and the amplitude is raised across the figure. The phase difference on the abscissa is plotted modulo $\pm\pi$; the ordinate is VCO input voltage. The loop finds the same limit cycle — period-one in parts (a) and (b), period-three in part (c) and period-two in part (d) — regardless of initial condition.

Fig. 10. Bifurcations and chaos in the phase-locked loop: (a) chaotic behavior at modulation frequency $\omega_E = 0.3\omega_{nat}$ (b) periodic behavior at $\omega_E = 0.4\omega_{nat}$ (c) chaotic behavior at $\omega_E = 0.5\omega_{nat}$ (d) chaotic behavior at $\omega_E = 0.6\omega_{nat}$. Same axes as the previous figure. Trajectories are sampled once per drive period and ϕ is plotted modulo $\pm\pi$. Damping ratio = 1/4 and modulation amplitude ratio = 1.2.

Fig. 11. A small segment of the trajectory that was sampled to produce part (c) of the previous figure.

Fig. 12. Parameter-space portrait of the phase-locked loop: C = chaotic; 1/2/3 = limit cycle with denoted period.

Fig. 13. Searching for a chaotic attractor that broadens the capture range: unlike the previous figures, the x-axis here is proportional to $\sin\phi$. The capture range is indicated by the two horizontal lines. The Poincaré section of the [amplitude ratio, frequency ratio] = [1.6, 0.3] attractor in part (a) does not quite touch the objective — the cross on the diagonal line. Raising the frequency ratio moves the attractor down and away from the objective; see part (b).

Raising the amplitude ratio moves the attractor towards — part (c) — and then past (part (d)) the cross. The parameter range between parts (c) and (d) is next examined more closely to determine the precise values that cause overlap to occur.

Fig. 14. The chaotic attractor found as a result of the search: amplitude ratio = 1.9 and frequency ratio = 0.3. The intersection of this attractor with the diagonal line that represents the locus of locked states surrounds the objective, making it — *and the range of frequencies that surrounds it* — reachable.